RESEARCH ARTICLE

WILEY

A numerical coupling scheme for nonlinear time history analysis of buildings on a regional scale considering site-city interaction effects

Xinzheng Lu[1] (iD) | Yuan Tian[2] | Gang Wang[3] | Duruo Huang[4]

[1] Key Laboratory of Civil Engineering Safety and Durability of China Education Ministry, Department of Civil Engineering, Tsinghua University, Beijing, P.R. China, 100084

[2] Beijing Engineering Research Center of Steel and Concrete Composite Structures, Tsinghua University, Beijing, China 100084

[3] Department of Civil and Environmental Engineering, Hong Kong University of Science and Technology, Clear Water Bay, Kowloon, Hong Kong

[4] Department of Hydraulic Engineering, Tsinghua University, Beijing, P.R. China 100084

Correspondence
Xinzheng Lu, Key Laboratory of Civil Engineering Safety and Durability of China Education Ministry, Department of Civil Engineering, Tsinghua University, Beijing, P.R. China, 100084.
Email: luxz@tsinghua.edu.cn

Funding information
National Natural Science Foundation of China, Grant/Award Number: No. 51578320; Hong Kong Research Grants Council, Grant/Award Number: GRF 16214118; HKUST Department of Civil and Environmental Engineering Intergroup Collaborative Research Program

Summary

Seismic damage simulation of buildings on a regional scale is important for loss estimation and disaster mitigation of cities. However, the interaction among densely distributed buildings in a city and the site, ie, the "site-city interaction (SCI) effects," is often neglected in most regional simulations. Yet, many studies have found that the SCI effects are very important in regional simulations containing a large number of tall buildings and underground structures. Therefore, this work proposed a numerical coupling scheme for nonlinear time history analysis of buildings on a regional scale considering the SCI effects. In this study, multiple-degree-of-freedom models are used to represent different buildings above the ground, while an open source spectral element program, SPEED, is used for simulating wave propagation in underlying soil layers. The proposed numerical scheme is firstly validated through a shaking table test. Then, a detailed discussion on the SCI effects in a 3D basin is performed. Finally, a nonlinear time history analysis of buildings on a regional scale is performed using the Tsinghua University campus in Beijing as a case study. The Tsinghua University campus case results show that the SCI effects will reduce the seismic responses of most buildings. However, some buildings will suffer much more severe damage when the SCI effects are considered, which may depend on the input motions, site characteristics, and building configurations.

KEYWORDS

multiple-degree-of-freedom model, regional seismic damage simulation, site-city interaction effect, SPEED, time history analysis

1 | INTRODUCTION

Earthquakes will cause a large amount of economic losses and casualties,[1-3] while a major part of seismic losses are contributed by building damages under earthquakes. Therefore, an accurate prediction of the seismic damage to buildings on a regional scale is important for city planning and postearthquake rescue, which will help mitigate direct/indirect seismic losses.[4-7]

Existing approaches for seismic damage evaluation of buildings on a regional scale mainly include the damage probability matrix method,[8,9] the capacity spectrum method,[5] and methods based on time history analysis (THA).[4,10] The damage probability matrix method relies greatly on historical damage data, which are not easily adopted for areas without sufficient statistical data. The capacity spectrum method can, to some extent, consider the seismic resistance

of individual buildings and the spectral characteristics of different ground motions. However, the effects of duration and pulse-like ground motions, or high-order vibration modes of buildings, cannot be fully considered by this method. Nowadays, the THA-based method has been widely used in regional seismic simulation with advancement in computer technology.[10,11] The THA-based method can take full consideration of the nonlinear dynamic characteristics of buildings as well as intensity, frequency content, and duration characteristics of ground motions, so it is particularly suitable for seismic damage simulation of buildings.[6,12] To balance the accuracy and efficiency of the THA-based regional scale simulation containing a large number of buildings, Lu et al[10] proposed a nonlinear multiple-degree-of-freedom (MDOF) shear model and a nonlinear multiple-degree-of-freedom flexural-shear model for different types of buildings. The accuracy and the efficiency of these nonlinear MDOF models have been systematically validated by comparing the simulation results with a number of experimental results using actual earthquake records.[13,14]

It is worth noting that, to date, the THA of buildings on a regional scale contains the following 2 steps: (1) the free-field ground motion is predicted by wave propagation modeling,[15] stochastic simulation,[16,17] or by using ground motion prediction equations and (2) the THA of buildings is performed to predict the seismic damage under the predicted free-field ground motions. In this way, the site effects might be well considered, but the soil-structure interaction (SSI) and the structure-soil-structure interaction (SSSI) would be neglected. Note that SSI and SSSI would change the motions around buildings (the so-called "Contamination of ground motions by buildings"). Particularly, for densely populated cities, a large amount of multistory and tall buildings are constructed closely to each other, which may greatly change the characteristics of sites. Such overall effects and the "global" interaction between all the buildings in a city and its subsoil are usually called "site-city interaction (SCI) effects."[18] Bard et al[18] found that "*if SCI effects turn out to be significant, one immediate consequence is that erecting or destroying a building, or a group of buildings, could modify seismic hazard for the neighbourhood, which in turn could lead to significant conceptual changes, especially concerning microzoning studies, land-use planning, and insurance policies.*" Recently, many theoretical, experimental, and numerical studies have been performed on the SCI effects.[11,18-34] For example, Schwan et al[31] reported a series of shaking table tests, and found that densely located buildings can greatly change the characteristics of the site and the dynamic responses of buildings; Semblat et al[32] performed the seismic wave propagation in an actual 2D shallow alluvial basin in Nice using boundary element method, and analyzed the influence of SCI effects; Isbiliroglu et al[24] analyzed the SCI effects of the Northridge Earthquake by using domain reduction method based on the Hercules system proposed by Tu et al.[35] Mazzieri et al[28] developed an open source program SPEED (SPectral Elements in Elastodynamics with Discontinuous Galerkin) using spectral element method, and performed the seismic simulation considering SCI effects for Christchurch, New Zealand.[36] The program is also used in a recent case study of SCI effects for an urban transportation hub in Hong Kong.[25]

Many existing studies proved that the ground motions can be affected by the existence of buildings, which may lead to a significant difference in the dynamic responses of buildings. For example, Isbiliroglu et al[24] found that the vibration of large-scale structures will greatly affect the nearby buildings; Guidotti et al[36] found that the SCI effects will change the ground motions by more than one-third compared with the free-field motions. Thus, the SCI effects should be well considered when conducting the seismic simulation of buildings on a regional scale.

Existing researches on SCI effects mainly focused on the wave propagation simulation. Instead, only very simple building models are adopted, such as elastic blocks, which are inaccurate and cannot consider the nonlinear behavior of real structures, and will lead to quite different simulation results from real structures. Therefore, based on existing studies, this work proposed a numerical coupling scheme for nonlinear THA of buildings on a regional scale considering the SCI effects. Multiple-degree-of-freedom models, which can accurately simulate the nonlinear dynamic behaviors of buildings, are used to represent the key features of different buildings above the ground. An open source spectral element program, SPEED, is used to compute the wave propagation in underlying soil layers. The proposed numerical scheme is firstly validated through a shaking table test. Then, a detailed discussion on the SCI effects in a 3D basin is performed. Finally, a nonlinear THA of buildings on a regional scale is performed using the Tsinghua University campus in Beijing as a case study. The SCI effects to the seismic damage of buildings and the feasibility of the proposed method are discussed.

2 | REGIONAL SCALE NONLINEAR THA OF BUILDINGS CONSIDERING SCI EFFECTS

2.1 | Nonlinear MDOF model for buildings above the ground

Lu et al[10] proposed that the nonlinear MDOF models can simulate the dynamic behavior of buildings with satisfactory accuracy and efficiency for regional seismic damage simulation. Therefore, the nonlinear MDOF models for buildings

(including MDOF shear models and MDOF flexural-shear models as shown in Figure 1A, B) and the corresponding parameter determination method proposed by Lu et al[10] and Xiong et al[13,14] are adopted in this work to perform the nonlinear THA of buildings on a regional scale.

In general, low-story and multistory buildings often exhibit shear deformation modes under earthquakes, while tall buildings will deform in flexure-shear modes. So the MDOF shear model will be used for the low-story and multistory buildings, and the MDOF flexural-shear model will be adopted to tall buildings. The masses of the buildings are concentrated on their corresponding stories, and the nonlinear behavior of the structure is represented by the nonlinear interstory force-displacement relationships. Thus, the parameter determination of the interstory force-displacement relationships will be very important for the rationality and accuracy of the simulation results, considering the limited available information for buildings on a regional scale.

Xiong et al[13,14] proposed a parameter determination and damage state determination method for the MDOF shear and flexural-shear models. In their work, trilinear backbone curves are adopted for the interstory force-displacement relationships (shown in Figure 1C), and a single parameter pinching model proposed by Steelman et al[37] is adopted. Firstly, based on building inventory data (including height, area, story number and so forth), a simulated design procedure is conducted according to the corresponding design codes, and the fundamental period and the design point on the backbone curve can be obtained. Then, according to related statistics of extensive experimental and analytical results, the yield point, peak point and softening point on the backbone curve can be further obtained, which in turn will determine the shape of the backbone curve. Five damage states, ranging from none, slight, moderate, to extensive, and complete damage, are considered in their work. The reliability of the proposed method is further validated by comparing simulation results with actual seismic response.

2.2 | SPEED for simulating the wave propagation in 3D site models

To conveniently simulate the SCI effects, an open source program, SPEED,[28] is adopted in this work. The program can simulate seismic wave propagation in 3-dimensional viscoelastic heterogeneous media on both local and regional scales. Based on the discontinuous Galerkin spectral approximation, SPEED can handle nonmatching grids in an efficient and versatile way, and has been successfully applied in many cases, such as Christchurch in New Zealand, Thessaloniki in Greece and so forth.[19,28,38,39]

The governing equation adopted in SPEED has the following expression to describe the wave propagation in the soil domain[28]:

$$\rho\ddot{\mathbf{u}} + 2\rho\xi\dot{\mathbf{u}} + \rho\xi^2\mathbf{u} - \nabla\cdot\boldsymbol{\sigma}(\mathbf{u}) = \mathbf{f} \tag{1}$$

where ρ is the density of the soil; $\mathbf{u}$, $\dot{\mathbf{u}}$, and $\ddot{\mathbf{u}}$ represent the displacement, velocity, and acceleration filed of the soil respectively; ξ is the decay factor; $\boldsymbol{\sigma}(\mathbf{u})$ is the Cauchy stress tensor; and $\mathbf{f}$ is the density of body forces. The explicit Newmark method ($\beta = 0$, $\gamma = 0.5$) is adopted for time integration in the dynamic simulation.

2.3 | Numerical coupling scheme for simulating SCI effects

Figure 2 illustrates the numerical coupling scheme for simulating SCI effects. The numerical scheme consists of 2 main parts. In the first part, wave propagation in the soil domain is solved by using SPEED via Equation (1). In the second
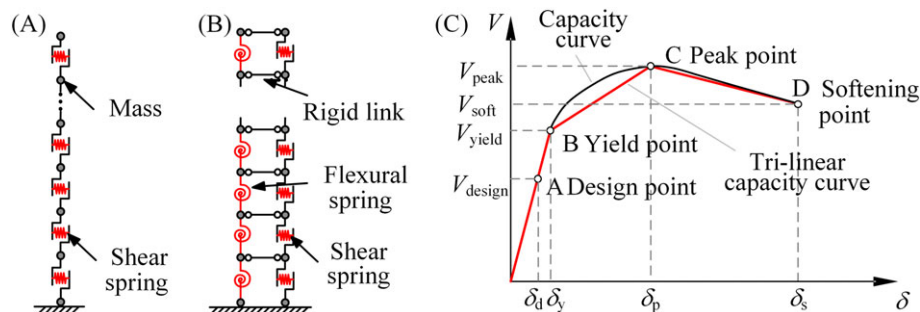

FIGURE 1 A, MDOF shear model. B, MDOF flexural-shear model. C, Trilinear backbone curve adopted in MDOF model[13,14] [Colour figure can be viewed at wileyonlinelibrary.com]
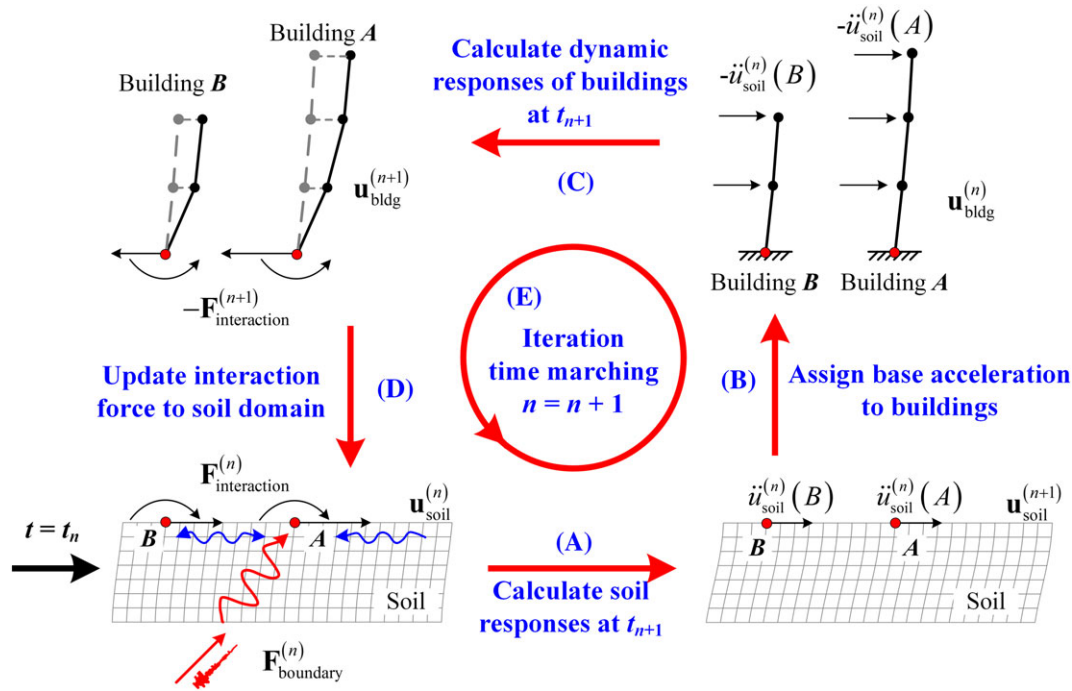
FIGURE 2 Numerical coupling scheme for SCI effects [Colour figure can be viewed at wileyonlinelibrary.com]

part, each building is modeled using the nonlinear MDOF model. To couple these 2 parts, in each time step, the base reaction forces from buildings are imposed to the soil domain, and the acceleration computed from the soil domain are set as base acceleration to buildings. The detailed computation procedure is illustrated in Figure 2 and shown as follows.

a. Given the soil response and boundary condition at t_n, the soil response at t_{n+1}, $\mathbf{u}_{\text{soil}}^{(n+1)}$, can be solved via Equation (1) by using explicit Newmark integration scheme ($\beta = 0, \gamma = 0.5$). The equation can be written in a matrix form for the whole soil domain as follows:

$$\left(\frac{1}{\Delta t^2} + \frac{\xi}{\Delta t}\right)\mathbf{M}_{\text{soil}}\mathbf{u}_{\text{soil}}^{(n+1)} = \mathbf{F}_{\text{ext,soil}}^{(n)} - \mathbf{F}_{\text{int,soil}}^{(n)} - \xi^2\mathbf{M}_{\text{soil}}\mathbf{u}_{\text{soil}}^{(n)} + \frac{\xi}{\Delta t}\mathbf{M}_{\text{soil}}\mathbf{u}_{\text{soil}}^{(n-1)} + \frac{1}{\Delta t^2}\mathbf{M}_{\text{soil}}\left(2\mathbf{u}_{\text{soil}}^{(n)} - \mathbf{u}_{\text{soil}}^{(n-1)}\right)$$

$$= \mathbf{F}_{\text{boundary}}^{(n)} + \mathbf{F}_{\text{interaction}}^{(n)} - \mathbf{F}_{\text{int,soil}}^{(n)} - \xi^2\mathbf{M}_{\text{soil}}\mathbf{u}_{\text{soil}}^{(n)} + \frac{\xi}{\Delta t}\mathbf{M}_{\text{soil}}\mathbf{u}_{\text{soil}}^{(n-1)} + \frac{1}{\Delta t^2}\mathbf{M}_{\text{soil}}\left(2\mathbf{u}_{\text{soil}}^{(n)} - \mathbf{u}_{\text{soil}}^{(n-1)}\right)$$

(2)

where the superscript represents the time step; the external load $\mathbf{F}_{\text{ext,soil}}^{(n)}$ applied to the soil domain at t_n consists of 2 different sources: $\mathbf{F}_{\text{boundary}}^{(n)}$ represents boundary forces for seismic wave input at the bottom and wave absorption at the sides of truncated soil domain, and $\mathbf{F}_{\text{interaction}}^{(n)}$ is the interaction force imposed to the soil domain at each building location, which can be easily calculated as the base reaction force of the building from dynamic structural analysis; $\mathbf{F}_{\text{int,soil}}^{(n)}$ denotes the internal load obtained from the soil response at t_n; $\mathbf{M}_{\text{soil}}$ is the mass matrix for the soil domain. Note that Equation (2) has considered not only the soil-structure interaction at the building location but also propagation and interaction of wave field because of inconsistency of soil motions at various locations, such that wave interaction among different building locations and wave interaction between the near field and the free field can be naturally captured. It is also worth mentioning that heterogeneous soil layers and complex 3D topography can also be modeled using the spectral element simulation.[15]

b. After obtaining the soil displacement field at t_{n+1}, the soil acceleration $\ddot{u}_{\text{soil}}^{(n)}$ at each building location (eg, A and B in Figure 2) at t_n can be assigned as base acceleration to each building using explicit Newmark method as shown in Equation (3).

$$\ddot{u}_{\text{soil}}^{(n)} = \frac{u_{\text{soil}}^{(n+1)} - 2u_{\text{soil}}^{(n)} + u_{\text{soil}}^{(n-1)}}{\Delta t^2} \tag{3}$$

c. In this work, dynamic response analysis is performed individually for each building using the nonlinear MDOF model shown in Figure 1. The nonlinear structural responses of each building at t_{n+1}, $\mathbf{u}_{\text{bldg}}^{(n+1)}$, can be obtained by solving Equation (4):

$$\left(\frac{1}{\Delta t^2}\mathbf{M}_{\text{bldg}} + \frac{1}{2\Delta t}\mathbf{C}_{\text{bldg}}\right)\mathbf{u}_{\text{bldg}}^{(n+1)} = -\mathbf{M}_{\text{bldg}}\{\mathbf{1}\}\ddot{u}_{\text{soil}}^{(n)} - \mathbf{F}_{\text{int,bldg}}^{(n)} + \frac{1}{2\Delta t}\mathbf{C}_{\text{bldg}}\mathbf{u}_{\text{bldg}}^{(n-1)} + \frac{1}{\Delta t^2}\mathbf{M}_{\text{bldg}}\left(2\mathbf{u}_{\text{bldg}}^{(n)} - \mathbf{u}_{\text{bldg}}^{(n-1)}\right) \tag{4}$$

where $\{\mathbf{1}\}$ stands for a vector of ones $\{1, 1, ..., 1\}^T$, $\mathbf{M}_{\text{bldg}}$ denotes the mass matrix of each building, $\mathbf{C}_{\text{bldg}}$ represents matrix for Rayleigh damping, and $\mathbf{F}_{\text{int,bldg}}$ denotes the internal force obtained from the nonlinear building analysis. It is noted that in solving the nonlinear structural responses, the base of each building (eg, A and B in Figure 2) is assumed to be fixed, and the base acceleration $\ddot{u}_{\text{soil}}^{(n)}$ is imposed as inertia force to each story. Hence, the term $\mathbf{u}_{\text{bldg}}$ in Figure 2 and Equation (4) represents the building's displacement relative to its base. As a result, the displacement compatibility at the building location is implicitly satisfied.

d. Taking the base reaction force from each building at t_{n+1} as the updated interaction force, the updated $\mathbf{F}_{\text{interaction}}^{(n+1)}$ is then applied to the soil domain at the building location for the next iteration.

e. Loop over steps (a) to (d) until the last time step.

To implement the above procedure, first of all, the building inventory data are necessary. The building inventory data include the height, story number, structural type, year built, location of the building, and other design information. The vibration period of the building is optional. If this information is not provided, the vibration period of the building will be estimated based on empirical equations and the building inventory data. Second, to update the interaction force $\mathbf{F}_{\text{interaction}}$ to the soil domain, the corresponding Neumann boundary conditions should be assigned according to the location of each building. A new function type for boundary conditions has been developed in SPEED, so that the boundary force can be updated at each time step by using the value of $\mathbf{F}_{\text{interaction}}$ calculated from the MDOF models.

Compared with existing models that simulate the SCI effects, the numerical coupling scheme proposed in this work requires only the building inventory data and the updated force boundary as additional input. The backbone curves of the buildings can be calculated automatically within the program according to Xiong et al's work,[13,14] which significantly reduces the workload of numerical modeling. The MDOF model can capture the nonlinear seismic response of buildings, which cannot be achieved if an elastic block model is used.[25] Owing to the reduced DOFs, the adoption of MDOF models for buildings is highly cost-effective for the simulation. The proposed method can not only consider the SSI at the building locations because of the coupling scheme but also the SSSI and SCI effects, because they have been naturally captured during the dynamic soil response simulation in SPEED.

3 | SHAKING TABLE TEST VALIDATION

A shaking table test[31] is simulated to validate the proposed numerical coupling scheme. The prototype of the shaking table test is shown in Figure 3A. A cellular polyurethane foam, with a size of 2.13 m × 1.76 m × 0.76 m ($X \times Y \times Z$), is used to simulate the underlying foundation. The polyurethane foam has a density of 49 kg/m³, damping ratio of 4.9%, shear velocity of 33 m/s, and Poisson ratio of 0.06. The fundamental frequency of the site in the X-direction is approximately 9.36 Hz according to the experimental measurement. Aluminum sheets with a height of 0.184 m and thickness of 0.5 mm are used to simulate multiple rows of buildings. The fundamental frequency of the aluminum sheets in the X-direction is approximately 8.45 Hz, with a damping ratio of approximately 4% according to the experimental results. The Ricker wavelet with spectral acceleration peak around 8 Hz is adopted as input signal to the bottom of the site. Two configurations, one having a single building, and the other having 37 buildings, are considered in the shaking table tests, as shown in Figure 3B.

To simulate this test, the site and the buildings are modeled separately. During the modeling procedure, the abovementioned parameters are adopted. The MDOF model with the same fundamental frequency, height, and mass
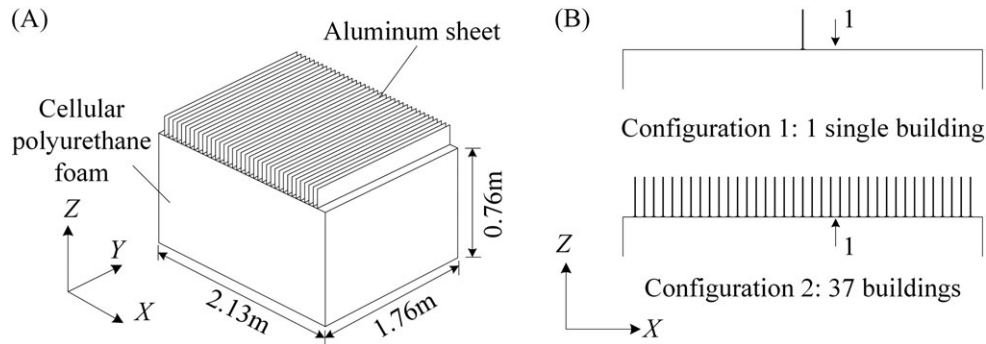
FIGURE 3 A, The prototype of the shaking table test. B, The configuration of buildings

is established, while the 3D solid model is adopted to simulate the site. The mesh used for the site model in the *X-Z* plane is shown in Figure 4. A mesh size of 93.75 mm is adopted along the *Z*-direction, and the mesh along the *X*-direction is determined according to the locations of the buildings. The first layer is established with a depth of 10 mm, so that the red part in Figure 4 can take the mass of the aluminum "foundations" (the aluminum angles at the bottom of the sheets) into consideration. The mesh size along the *Y*-direction is 0.05 m. A polynomial degree of 2 is adopted for the site model. Considering the shear velocity of the site (33 m/s) and the frequency range considered in this simulation (5-20 Hz), the average number of points per minimum wavelength is greater than 5; this shows that the mesh size adopted in this work can be considered to be reasonable.[40] Based on the established model, the Ricker wavelet is adopted as the Dirichlet boundary condition at the bottom surface of the site model. During computation, the ground motions recorded at point 1 and the corresponding transfer functions with respect to the input motion at the bottom of the site are compared, as shown in Figures 5 and 6.

Figures 5 and 6 show that the SCI effects will become more significant when the density of buildings is larger. The characteristics of the site can hardly be changed by only 1 building. But when the number of buildings is large enough, the SCI effects will lead to a smaller fundamental frequency of the site. In addition, 2 modes appear in the transfer function with smaller amplitudes (Figure 6B) instead of only 1 large peak (Figure 6A). The comparison between the
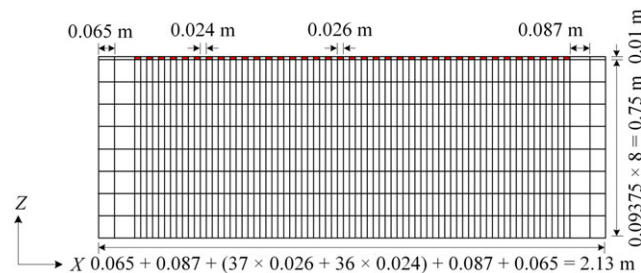

FIGURE 4 Meshing scheme of the site model [Colour figure can be viewed at wileyonlinelibrary.com]
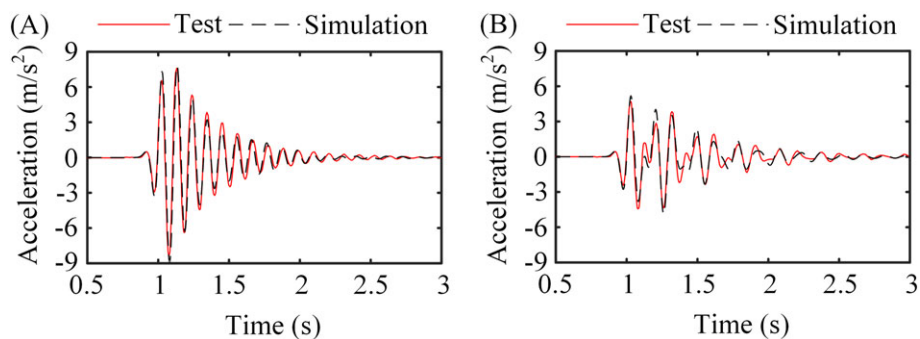

FIGURE 5 Comparison of the ground motions at point 1 under Configuration 1 A, and Configuration 2 B [Colour figure can be viewed at wileyonlinelibrary.com]
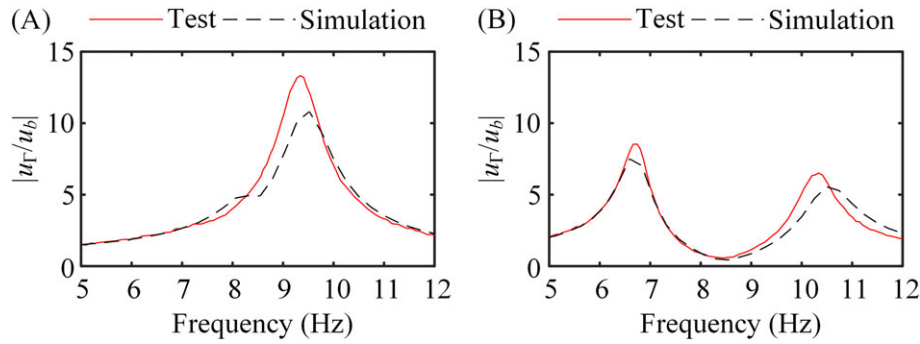
FIGURE 6 Comparison of the transfer function $|u_\Gamma/u_b|$ under Configuration 1 A, and Configuration 2 B [Colour figure can be viewed at wileyonlinelibrary.com]

simulation and test results demonstrate that the numerical coupling scheme proposed in this study can rather accurately simulate the influence of the SCI effects.

4 | CASE STUDY OF SCI EFFECTS IN A 3D BASIN

4.1 | The model setup

Because of focusing effects, earthquake ground motions are often greatly amplified within a basin. In addition, double resonance may occur if the fundamental period of a basin is close to that of the structure. Under double resonance conditions, the SCI effects will be very significant according to previous studies.[26,32] In this section, the method proposed in Section 2 will be adopted to perform a case study on the SCI effects in a 3D basin. To make full use of existing research outcomes, the trapezoidal (TRP) basin model analyzed by Sahar et al[30] is adopted in this study. The buildings are considered to be elastic, and the Ricker wavelet is used in the simulation. Note that, when detailed building inventory data are available, the numerical coupling scheme proposed in this study can simulate the nonlinear dynamic behavior of buildings, which will be shown in Section 5.

In this case, the size of the site considered is 3 km × 3 km with a depth of 600 m. A TRP basin with a maximum depth of 150 m is located at the center of the site. The slope of the inclined base of the TRP basin is 30°, and the detailed dimensions can be found in Figure 7. The rest of the site is made of rock, while the bottom layer with a depth of 100 m is used for plane wave input. The parameter of the site media is shown in Table 1. On the center of the basin surface, 9 building groups (denoted as B1 to B9) are arranged as 3 × 3, while the centers of each building group on the surface are denoted as P1 to P9 as shown in Figure 8. The distance between neighboring building groups is 52 m. Each building group contains 9 buildings arranged as 3 × 3 with a distance of 28 m. The width and length of each building is 56 m, while the story height of each building is 3 m. The number of stories for these buildings varies in this case study.

The fundamental frequency of the basin is approximately 0.6 Hz according to the soil parameters of the basin. Thus, the Ricker wavelet with a dominant frequency of 0.6 Hz is adopted as the input motion along the X-axis. To achieve the double resonance condition, 16-story buildings (with a fundamental frequency of 0.625 Hz) are placed on the ground
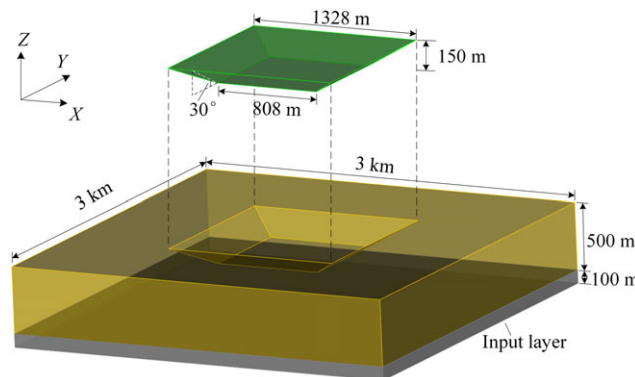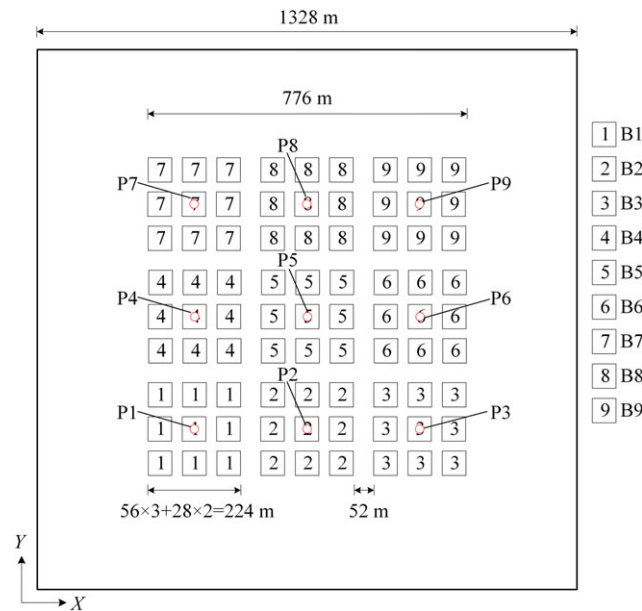

FIGURE 7 The dimension of the TRP Basin model [Colour figure can be viewed at wileyonlinelibrary.com]

TABLE 1 Parameters of the basin and rock[30]

Material	Density (kg/m³)	V_S (m/s)	V_P (m/s)	Q_S[a]	Q_P
Basin	1800	360	612	36	61
Rock	2650	1800	3060	180	300

[a]The Q factor determines the qualitative behavior of damped oscillators. It equals $1/(2\zeta)$, where ζ is the damping ratio.[41]

FIGURE 8 The building configuration [Colour figure can be viewed at wileyonlinelibrary.com]

surface of the basin. For comparison, buildings in several building groups are replaced by 8-story buildings, while the building locations are still the same, so that the influence of the height/frequency of the buildings on the SCI effect can be well simulated.

Three cases are simulated and discussed in this study:

Case 1: The seismic wave propagation in the site is simulated under free-field condition. And the building responses are simulated based on the free-field motions.

Case 2: The SCI effects are considered during the computation, while all the buildings are 16-story buildings (denoted as Configuration A). This case is also a double resonance condition.

Case 3: The SCI effects are also considered during the computation, while the buildings in the B2, B4, B6, and B8 groups are replaced by 8-story buildings (denoted as Configuration B).

The motions on the basin surface are recorded, and the ground motions at P1 to P9 will be analyzed in detail.

4.2 | Case 1: building response under free-field motion without SCI effects

The peak ground acceleration and velocity (PGA and PGV) on the surface of the basin under Ricker wavelet are shown in Figures 9 and 10. Case 1 simulated the free-field situation, in which no building is on the surface of the basin. However, the locations of buildings are also marked by white lines for the convenience of discussions in the following sections. Figures 9 and 10 show that, under the free-field condition, although the Ricker wavelet is input along the X-axis, there are also ground motions along the Y-axis because of the reflection at the basin boundaries. At the same time, because of the symmetry of the site, the distribution of PGA and PGV is also symmetrical. In general, the center of the basin has the highest level of PGA and PGV. In addition, there are 3 peaks of the intensity (PGA and PGV)
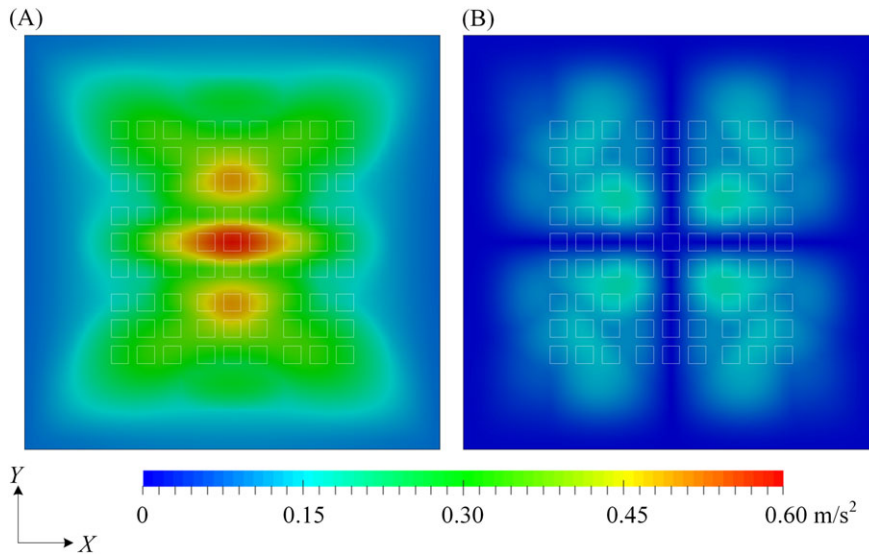
(A)   (B)

FIGURE 9 Distribution of PGA under the free-field condition (Case 1) along the X-axis A, and Y-axis B [Colour figure can be viewed at wileyonlinelibrary.com]
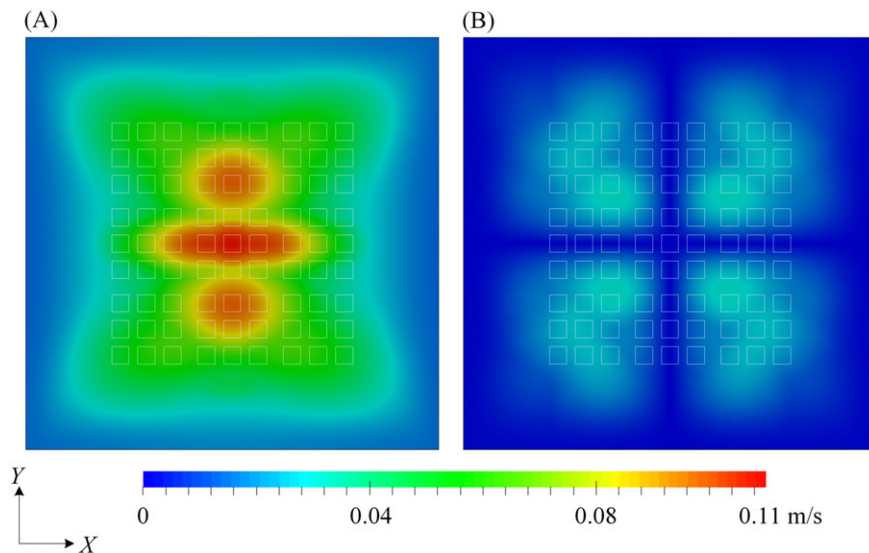
Y
└→ X

0   0.15   0.30   0.45   0.60 m/s²

(A)   (B)

FIGURE 10 Distribution of PGV under the free-field condition (Case 1) along the X-axis A, and Y-axis B [Colour figure can be viewed at wileyonlinelibrary.com]

Y
└→ X

0   0.04   0.08   0.11 m/s

distribution along the Y-axis, with a distance of approximately 192 m. Because of the similar pattern of PGA and PGV, the following sections will only discuss the differences of PGA distribution among the 3 cases in detail.

The transfer functions of the ground motions at P1 to P9 with respect to the input motion can be further obtained from the simulation. Because of the symmetry of the results, the transfer functions at (P1, P3, P7, and P9), (P2 and P8), and (P4 and P6) are also the same (results of Case 2 and Case 3 in the following section also have the same conclusions). Therefore, only the transfer functions at P1, P2, P4, and P5 will be discussed. The transfer functions and response spectrum of ground motions at P1, P2, P4, and P5 are shown in Figure 11. According to Figure 11, the fundamental period of the basin is approximately 0.66 Hz, but different ground motions at different locations show different characteristics. In general, peak transfer functions are located in 4 frequency bands around 0.66 Hz, 0.78 to 0.80 Hz, 1.00 to 1.07 Hz, and 1.29 to 1.39 Hz.

Existing THA of buildings on a regional scale directly input the free-field motions to the buildings for THA. Thus, both of the buildings in configurations A and B are analyzed by inputting the free-field motions obtained at their locations. The maximum roof drift ratio (RDR) of each building can be obtained as shown in Figure 12. For Configuration A, all of the 81 buildings have the same properties, so their responses are approximately proportional to the intensity (PGA) of the input motions. By contrast, for Configuration B, buildings in B2, B4, B6, and B8 are replaced by 8-story buildings, which in turn show smaller responses.
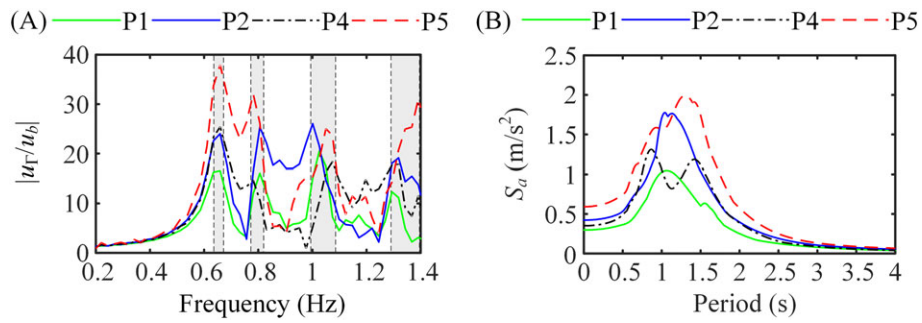
FIGURE 11 Transfer function A, and response spectrum B, results at P1, P2, P4, and P5 in Case 1 [Colour figure can be viewed at wileyonlinelibrary.com]
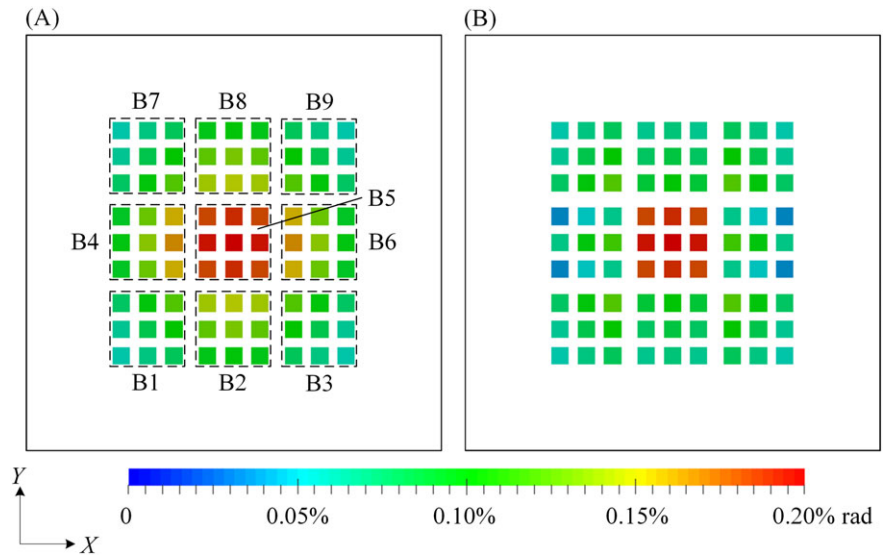

FIGURE 12 The maximum RDR along the X-axis of buildings in Configuration A A, and B B, under free-field ground motions (Case 1) [Colour figure can be viewed at wileyonlinelibrary.com]

4.3 | Case 2 and Case 3: building response considering SCI effects

Based on the numerical coupling scheme proposed in Section 2, the SCI effects are simulated in Case 2 and Case 3. Note that the PGV results have a very similar pattern with PGA results, so only PGA results will be discussed. The distribution of PGA on the surface of TRP basin under Ricker wavelet (with a dominant frequency of 0.6 Hz) is shown in Figure 13. The same legends are adopted as those in Figure 9, so that the influence caused by SCI effects can be
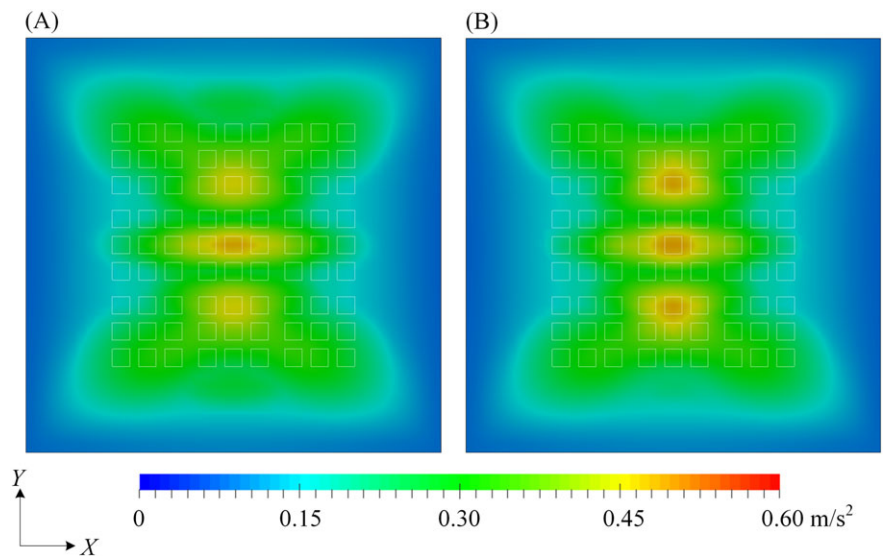

FIGURE 13 PGA distribution in Case 2 A, and Case 3 B, along the X-axis considering SCI effects [Colour figure can be viewed at wileyonlinelibrary.com]

illustrated easily. Because the ground motions are mainly along the *X*-axis, the results along the *Y*-axis will not be discussed. Compared with the results under free-field condition, the SCI effects will greatly reduce the surface motion intensity under the double resonance condition, which agrees with previous studies.[29,32]

The increase ratios of PGA with respect to the results in Case 1 (free-field condition) can be obtained, and are further shown in Figure 14 (Negative values mean reduction). The intensity of ground motions on the surface of the basin is generally reduced by the SCI effects with a maximum reduction of 24.98%. Further study shows that the SCI effects can be very complex. For Case 2, all of 81 buildings on the surface of the basin are 16-story buildings. The reduction region of PGA has an elliptical shape, and the maximum reduction is located at the center of the ellipse, while some fluctuation exists in local areas. In addition, because of the reflection from the boundary of the basin and the wave radiated from buildings, the regions near building blocks along the *Y*-axis (denoted as R1 and R2 in Figure 14A) also have some intensity reductions. In Case 3, buildings in B2, B4, B6, and B8 are replaced by 8-story buildings, which results in more complex results. The locations of B1 to B9 have been illustrated in Figure 14A. The PGA in B2 and B8 are hardly influenced by the SCI effects, with a reduction ratio of less than 10%. But in B4 and B6, more reductions in ground motion intensity are caused than those of Case 2. Similar to the results in Case 2, there are also some regions near the building blocks along the *Y*-axis where the intensity is greatly reduced. But Case 3 has more reductions than Case 2. Comparing results between Case 2 and Case 3, it can be found that the ground motions can also be influenced by the height/frequency of buildings, though the building density is the same.

Figure 15 shows the increase ratio of maximum RDR of buildings in Case 2 and Case 3 considering SCI effects compared with Case 1. Compared with the results in Figure 14, it can be found that the building responses are influenced by the SCI effects in a similar way with the intensity of ground motions (PGA). In Case 2, the maximum reduction of RDR can be larger than 25% (25.91%); while in Case 3, the maximum reduction of RDR is less than 20% (18.82%). In general, the responses of buildings located at the middle row along *X*-axis will be influenced most significantly by the SCI effects because of the shape of the TRP basin.

In addition, the characteristics of the TRP basin can be studied from the outputs at P1 to P9. Considering the symmetry of results, only the results of P1, P2, P4, and P5 will be discussed. The comparison of the response spectrum of the ground motions at these points and the comparison of their transfer functions with respect to the input motion are shown in Figures 16 and 17. Note that the fundamental frequencies of the 16-story and 8-story buildings are 0.625 and 1.25 Hz respectively. For Case 2, the transfer function values near the fundamental frequency of buildings (0.625 Hz) are greatly reduced, with a reduction of peak frequency as well (because of the inertia effect of buildings on the surface of the basin). The transfer function values in higher frequency range will also be reduced a bit. For Case 3, because the buildings located at P2 and P4 are 8-story buildings, the corresponding transfer function values will be further reduced around the frequency of 1.25 Hz. In addition, the fundamental frequency of the basin is also reduced because of the inertia effect, with a smaller amplitude as well. But the reduction of transfer function values is less than those in Case 2.
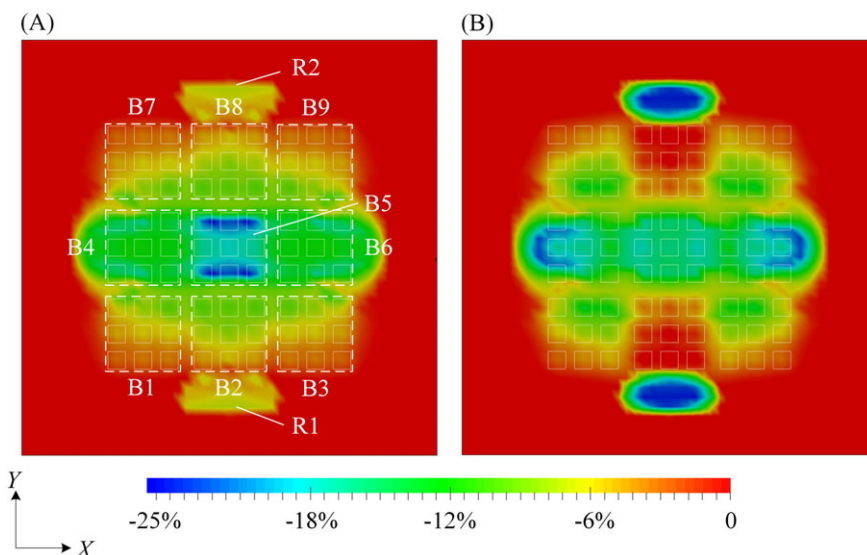

FIGURE 14 Increase ratio of PGA on the surface of the basin in Case 2 A, and Case 3 B, compared with Case 1 (negative value means reduction) [Colour figure can be viewed at wileyonlinelibrary.com]

FIGURE 15 Increase ratio of maximum RDR along the X-axis of buildings in Case 2 A, and Case 3 B, when considering SCI effects (negative value means reduction) [Colour figure can be viewed at wileyonlinelibrary.com]
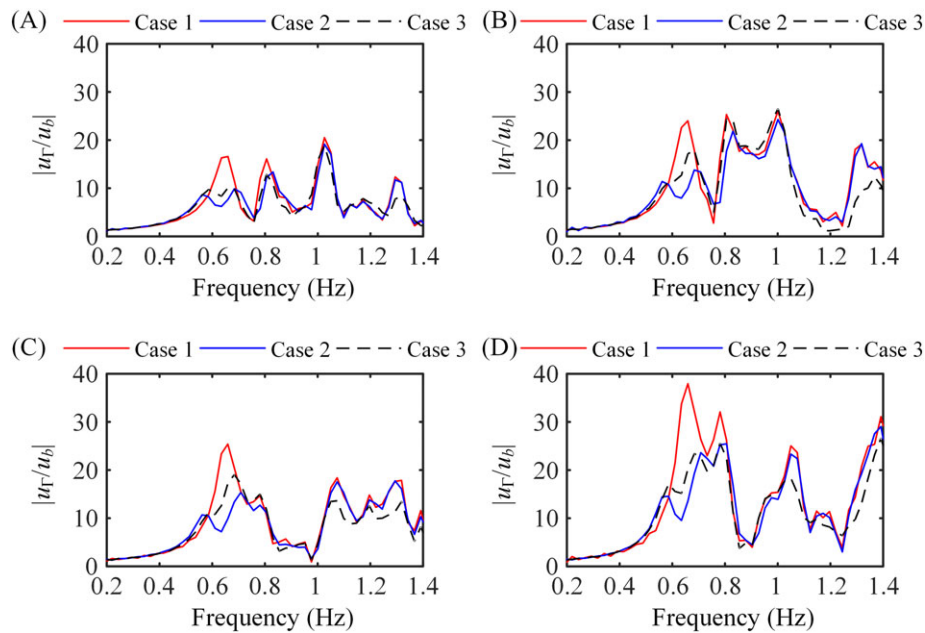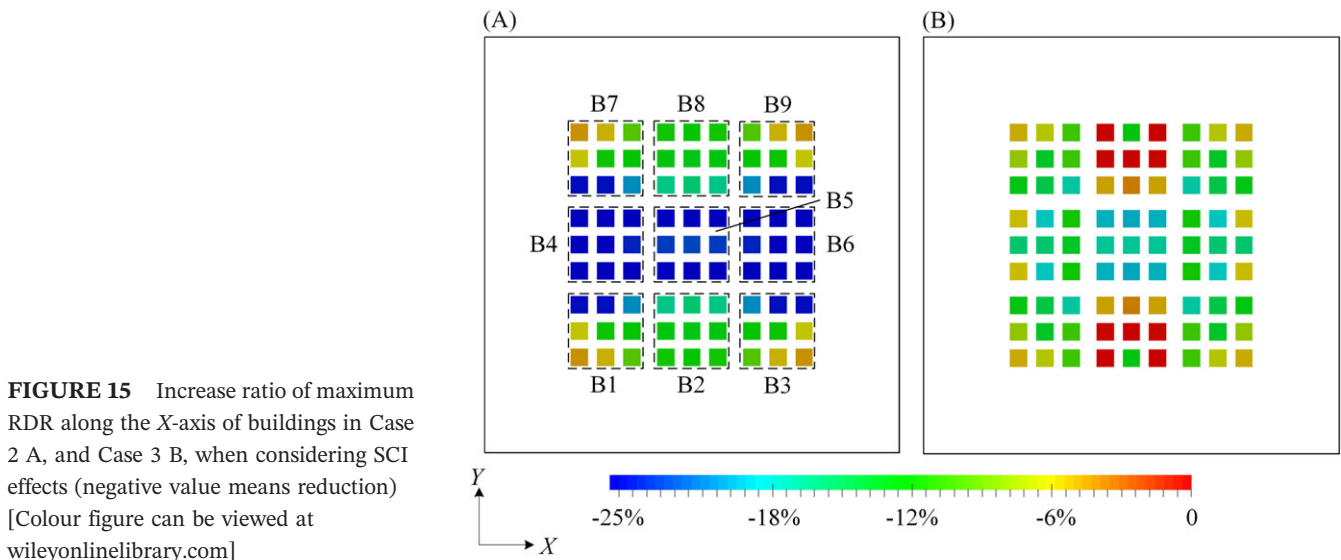

FIGURE 16 Comparison of the transfer function results at P1 A, P2 B, P4 C, and P5 D, with/without SCI effects [Colour figure can be viewed at wileyonlinelibrary.com]

Figure 17 shows that the response spectrum of ground motions on the surface of the basin is generally reduced by the SCI effects. But it is also worth noting that the response spectrum value of P2 in Case 3 at the period of 1.2 s is larger than that in Case 1 (free-field condition), which also reminds us that the response of buildings can also become larger because of SCI effects considering the complicated dynamic features of buildings and sites in real world.

According to above discussion, it can be found that for the 3D TRP basin studied in this section:

(1) Under the double resonance condition (Case 2), the responses of buildings and the site will be reduced, which has been found in previous studies.[29,32] The method proposed in this work can fully represent this phenomenon caused by SCI effects. As a result, traditional seismic damage simulation of buildings on a regional scale (the free-field motions are inputted directly to buildings) is conservative. However, it should be noted that, different from conventional design procedures (a conservative design is acceptable), a conservative prediction will overestimate the damage of buildings, which may in turn influence the distribution of relief supplies, and further restrict the
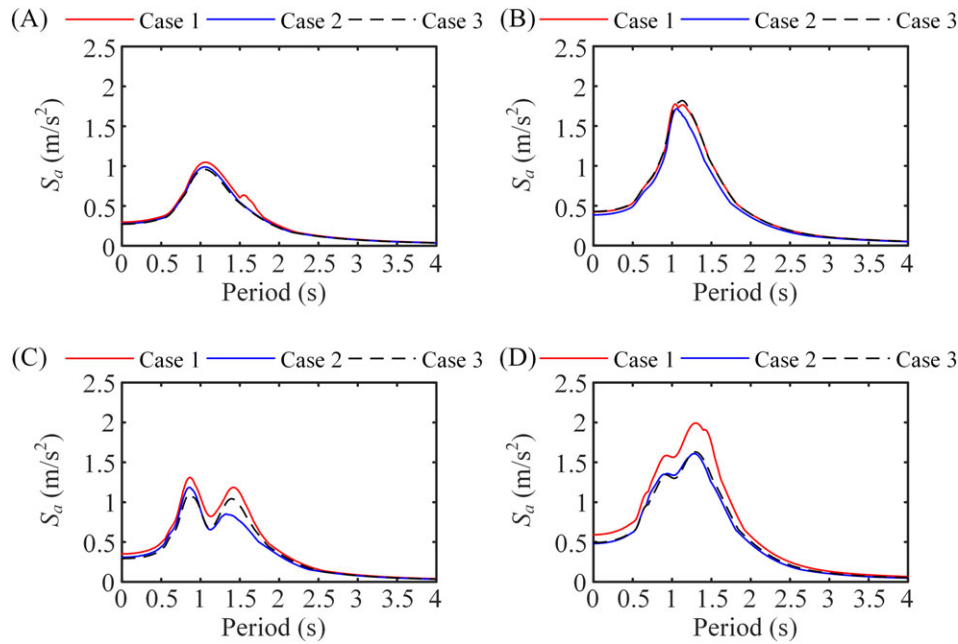
FIGURE 17 Comparison of the spectral acceleration results at P1 A, P2 B, P4 C, and P5 D, with/without SCI effects [Colour figure can be viewed at wileyonlinelibrary.com]

efficiency of postearthquake rescue work. Thus, it is of great value to take consideration of SCI effects in the seismic damage simulation of buildings.

(2) The existence of buildings will reduce the fundamental frequency of the site, and the transfer function amplitudes at the fundamental frequencies of both the buildings and the site will be reduced.

(3) Wave propagation in a basin can be quite complicated, and the reflection at the boundary of the basin will greatly influence the ground motions at the ground surface. Even if the building density on the surface of the basin keeps the same, the change of the building height/frequency will also significantly influence the SCI effects. Thus, the building density alone is not sufficient for measurement of SCI effects.

5 | CASE STUDY OF TSINGHUA UNIVERSITY CAMPUS

5.1 | Introduction of the campus model

The Tsinghua University campus at Beijing is used to study the influence of SCI effects on the seismic damage simulation of buildings on a regional scale. The size of the region considered is 3 km × 3 km × 350 m (length × width × depth). Based on geological investigations and literature, the soil condition of the site is defined as follows:

(1) The thickness of the Quaternary deposits is 100 m,[42] where the soil density is 2000 kg/m^3.

(2) The thickness of the Tertiary deposits is 100 m,[43] with a density of 2350 kg/m^3.

(3) The shear velocity, V_S, varies linearly from 200 m/s on the ground surface to 300 m/s in the depth of 30 m,[44] and 1000 and 1800 m/s at the bottom of the Quaternary and Tertiary deposits respectively.[43] The shear velocity profile is shown in Figure 18A;

(4) The bottom layer of the site is made of rock with a density of 2700 kg/m^3 and a shear velocity of 3400 m/s.[43] In the simulation, the bedrock is truncated at 150 m in thickness.

By inputting the Ricker wavelet (with a dominant frequency of 2 Hz) to the bottom of the site model, the transfer function of the site (free filed motions with respect to input motions at the bedrock) is shown in Figure 18B, where the wave amplification peaks up at 1.2, 2.5, and 4.0 Hz.
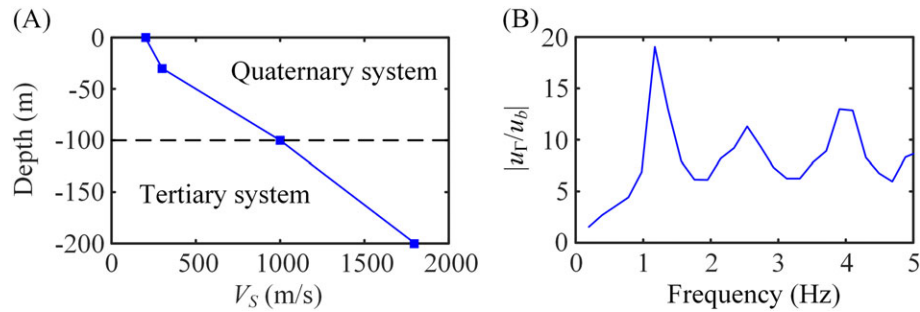
FIGURE 18 A, The distribution of the shear velocity. B, The transfer function of the site [Colour figure can be viewed at wileyonlinelibrary.com]

5.2 | Seismic simulation of buildings considering SCI effects

Based on previous building survey data,[3] 619 buildings in Tsinghua University campus are considered. Corresponding MDOF models of buildings can be obtained according to the work by Xiong et al.[13,14]

In this study, the Sanhe-Pinggu Earthquake (M8.0) scenario is considered, where Tsinghua University campus is located approximately 50 km to the earthquake epicenter. The target free-field ground motion is simulated and provided by the China Earthquake Administration[43] according to the scenario, as shown in Figure 19A. The SHAKE program[45] is used to perform the deconvolution of the ground motion to the bottom of the site, as shown in Figure 19B.

Based on the site model and the input motion mentioned above, 2 cases are performed:

Case T1 The free filed motion is used directly as the input motion of the buildings, without considering the SCI effects.
Case T2 The proposed numerical coupling scheme is adopted to simulate wave propagation and interaction between the buildings and the site.

As demonstrated in Section 4, although Case T1 is usually adopted in seismic simulation of buildings on a regional scale, it does not consider the SCI effects, which may lead to different responses of buildings. So Case T2 is performed to study the influence of the SCI effects on the responses of buildings. Figure 20 shows the increase ratio of maximum RDR of buildings considering SCI effects and corresponding decomposition.

Further study shows that the consideration of the SCI effects will generally reduce the roof drift of buildings by 6.59% on average, while the maximum reduction can reach 45.72% and the maximum increase can be more than 50%. For most buildings, the increase/reduction ratio is no more than 25% (as shown in Figure 20B). However, 10 buildings, which are all unreinforced masonry buildings, suffer a large increase of roof drift for more than 50% because of low seismic resistances and ductility of these buildings, as small increase in ground motion will induce large increase in roof displacement responses. For example, Building No. 559 is a 3-story unreinforced building. The backbone curve for the first floor of the building is shown in Figure 21A. The response spectrum comparison of the motions at the structure location in the 2 cases is shown in Figure 21B. The interstory drift ratio (IDR) responses of the first floor of Building No. 559 in Cases T1 and T2 are shown in Figure 21C. The difference between the motions in Figure 21B is far smaller than the responses in Figure 21C. This is because the interstory shear-drift relationship of the building has reached the
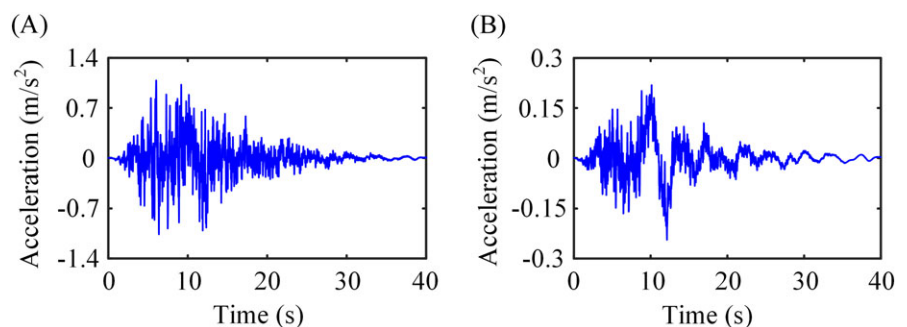

FIGURE 19 A, The free-field ground motion. B, The deconvoluted motion at the bottom of the site [Colour figure can be viewed at wileyonlinelibrary.com]
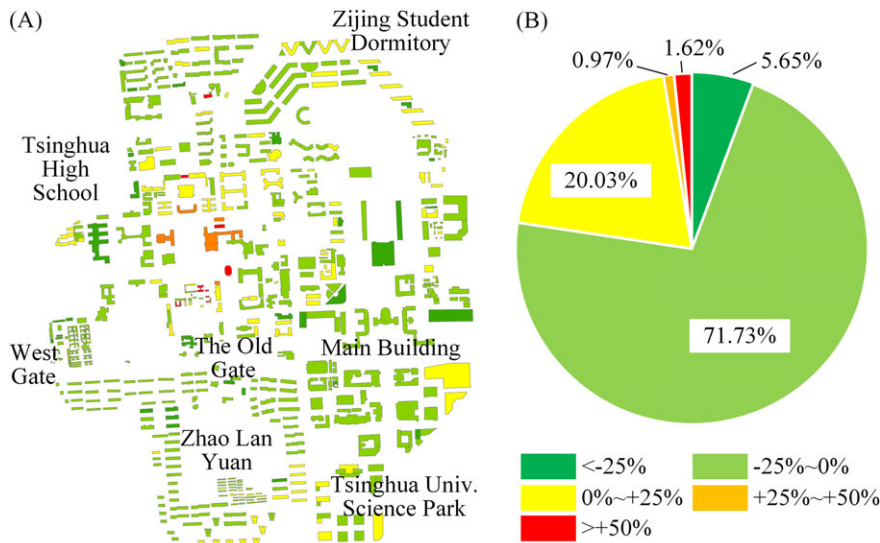
(A)

(B)

FIGURE 20 A, The distribution of increase ratio of maximum RDR. B, The composition of increase ratio of maximum RDR [Colour figure can be viewed at wileyonlinelibrary.com]
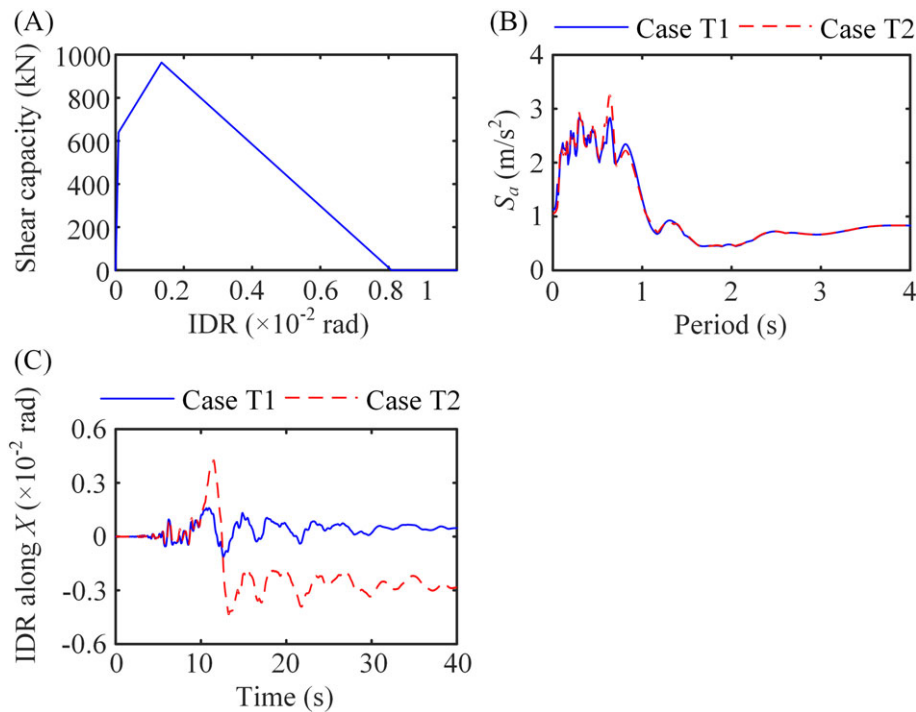

FIGURE 21 A, The backbone curve of the first floor in Building No. 559. B, Comparison of response spectrum. C, Comparison of IDR responses of the 1st floor in Building No. 559 [Colour figure can be viewed at wileyonlinelibrary.com]

descending part of the backbone curve at approximately 10 s (the peak IDR of the backbone curve is 0.0013). At this moment, a small fluctuation of the input motion will collapse the first floor, and further lead to a much larger roof drift response.

From the distributions provided in Figure 20A, the mechanism of SCI effects can be very complex, because of the building distribution, the characteristics of the site, and the input motions. From this case, the SCI effects will reduce the responses of most buildings. However, more severe damage occurs to several buildings. Such severe damage may lead to significant casualties. Therefore, the SCI effects should be well considered when performing nonlinear THA of buildings on a regional scale.

6 | CONCLUSIONS

A numerical coupling scheme based on the MDOF models and the SPEED program is proposed in this work to simulate the SCI effect. The proposed method has been validated and successfully applied to the 3D basin site and Tsinghua University campus case study. Several conclusions can be drawn as follows:

(1) The validation of the shaking table test shows that the proposed numerical scheme can simulate the influence of the SCI effects with a satisfactory accuracy.
(2) Under the double resonance condition, the responses of buildings and the site will be greatly reduced, which has been found in previous studies. The method proposed in this work can fully represent this characteristics caused by SCI effects.
(3) From the case study of the 3D basin, the building density alone is not sufficient for measuring the SCI effects. Some other factors, such as the building height and input motions, need to be considered together as well.
(4) In the case study of Tsinghua University campus, the SCI effects will generally reduce the structural responses. But some buildings may suffer more severe damage because of the SCI effects and the nonlinear behavior of buildings. Thus, the SCI effects should be well considered during the nonlinear THA of buildings on a regional scale.
(5) The mechanism of SCI effects can be very complex, which will be greatly influenced by the building configuration, site characteristics, input motions, and so forth. The numerical scheme proposed in this work can provide a useful simulation tool to researches on SCI effects, and more generalized conclusions will be discussed in the future.

ORCID

Xinzheng Lu ![ORCID] http://orcid.org/0000-0002-3313-7420

REFERENCES

1. Guha-Sapir D, Vos F, Below R, Ponserre S. *Annual disaster statistical review 2010: the numbers and trends. Centre for Research on the Epidemiology of Disasters (CRED).* Brussels, Belgium: Université catholique de Louvain; 2011.
2. Guha-Sapir D, Vos F, Below R, Ponserre S. *Annual disaster statistical review 2011: the numbers and trends. Centre for Research on the Epidemiology of Disasters (CRED).* Brussels, Belgium: Institute of Health and Society (IRSS), Université catholique de Louvain; 2012.
3. Zeng X, Lu XZ, Yang T, Xu Z. Application of the FEMA-P58 methodology for regional earthquake loss prediction. *Nat Hazards.* 2016;83(1):177-192.
4. Hori M. *Introduction to computational earthquake engineering.* London: Imperial College Press; 2006.
5. FEMA. *Multi-hazard loss estimation methodology: earthquake model (HAZUS-MH 2.1 technical manual).* Washington, DC: Federal Emergency Management Agency; 2012.
6. Lu XZ, Han B, Hori M, Xiong C, Xu Z. A coarse-grained parallel approach for seismic damage simulations of urban areas based on refined models and GPU/CPU cooperative computing. *Adv Eng Software.* 2014;70:90-103.
7. FEMA. *P-366. Hazus® estimated annualized earthquake losses for the United State.* Washington, DC: Federal Emergency Management Agency; 2017.
8. ATC-13. Earthquake damage evaluation data for California. Redwood City, California: Applied Technology Council, 1985.
9. Yakut A, Ozcebe G, Yucemen MS. Seismic vulnerability assessment using regional empirical data. *Earthquake Eng Struct Dyn.* 2006;35(10):1187-1202.
10. Lu XZ, Guan H. *Earthquake disaster simulation of civil infrastructures: from tall buildings to urban areas.* Singapore: Springer; 2017.
11. Hori M, Ichimura T. Current state of integrated earthquake simulation for earthquake hazard and disaster. *J Seismol.* 2008;12(2):307-321.

12. Lu XZ, Tian Y, Guan H, Xiong C. Parametric sensitivity study on regional seismic damage prediction of reinforced masonry buildings based on time-history analysis. *Bull Earthquake Eng*. 2017;15(11):4791-4820.

13. Xiong C, Lu XZ, Guan H, Xu Z. A nonlinear computational model for regional seismic simulation of tall buildings. *Bull Earthquake Eng*. 2016;14(4):1047-1069.

14. Xiong C, Lu XZ, Lin XC, Xu Z, Ye LP. Parameter determination and damage assessment for THA-based regional seismic damage prediction of multi-story buildings. *J Earthquake Eng*. 2017;21(3):461-485.

15. Wang G, Du C, Huang D, Jin F, Koo RCH, Kwan JSH. Parametric models for 3D topographic amplification of ground motions considering subsurface soils. *Soil Dyn Earthquake Eng*. 2018; in press. https://doi.org/10.1016/j.soildyn.2018.07.018

16. Huang D, Wang G. Stochastic simulation of regionalized ground motions using wavelet packet and cokriging analysis. *Earthquake Eng Struct Dyn*. 2015;44(5):775-794.

17. Huang D, Wang G. Energy-compatible and spectrum-compatible (ECSC) ground motion simulation using wavelet packets. *Earthquake Eng Struct Dyn*. 2017;46(11):1855-1873.

18. Bard PY, Chazelas J, Guéguen P, Kham M, Semblat JF. Site-city interaction. In: *Assessing and Managing Earthquake Risk*. Dordrecht: Springer; 2006:91-114.

19. Abraham JR, Smerzini C, Paolucci R, Lai CG. Numerical study on basin-edge effects in the seismic response of the Gubbio valley, Central Italy. *Bull Earthquake Eng*. 2016;14(6):1437-1459.

20. Boutin C, Soubestre J, Schwan L, Dietz M. Multi-scale modeling for dynamics of structure-soil-structure interactions. *Acta Geophys*. 2014;62(5):1005-1024.

21. Ghergu M, Ionescu IR. Structure-soil-structure coupling in seismic excitation and "city effect". *Int J Eng Sci*. 2009;47(3):342-354.

22. Groby JP, Wirgin A. Seismic motion in urban sites consisting of blocks in welded contact with a soft layer overlying a hard half-space. *Geophys J Int*. 2008;172(2):725-758.

23. Hans S, Boutin C, Ibraim E, Roussillon P. In situ experiments and seismic analysis of existing buildings. Part I: experimental investigations. *Earthquake Eng Struct Dyn*. 2005;34(12):1513-1529.

24. Isbiliroglu Y, Taborda R, Bielak J. Coupled soil-structure interaction effects of building clusters during earthquakes. *Earthq Spectra*. 2015;31(1):463-500.

25. Kato B, Wang G. Ground motion simulation in an urban environment considering site-city interaction: a case study of Kowloon station, Hong Kong. In: *3rd Huixian International Forum on Earthquake Engineering for Young Researchers*. University of Illinois, Urbana-Champaign, United States, August 11–12, 2017.

26. Kham M, Semblat JF, Bard PY, Dangla P. Seismic site–city interaction: main governing phenomena through simplified numerical models. *Bull Seismol Soc Am*. 2006;96(5):1934-1951.

27. Lou M, Wang H, Chen X, Zhai YM. Structure-soil-structure interaction: literature review. *Soil Dyn Earthquake Eng*. 2011;31(12):1724-1731.

28. Mazzieri I, Stupazzini M, Guidotti R, Smerzini C. SPEED: SPectral Elements in Elastodynamics with Discontinuous Galerkin: a non-conforming approach for 3D multi-scale problems. *Int J Numer Methods Eng*. 2013;95(12):991-1010.

29. Sahar D, Narayan JP, Kumar N. Study of role of basin shape in the site–city interaction effects on the ground motion characteristics. *Nat Hazards*. 2015;75(2):1167-1186.

30. Sahar D, Narayan JP. Quantification of modification of ground motion due to urbanization in a 3D basin using viscoelastic finite-difference modelling. *Nat Hazards*. 2016;81(2):779-806.

31. Schwan L, Boutin C, Padrón LA, Dietz MS, Bard PY, Taylor C. Site-city interaction: theoretical, numerical and experimental crossed-analysis. *Geophys J Int*. 2016;205(2):1006-1031.

32. Semblat JF, Kham M, Bard PY. Seismic-wave propagation in alluvial basins and influence of site-city interaction. *Bull Seismol Soc Am*. 2008;98(6):2665-2678.

33. Tsogka C, Wirgin A. Simulation of seismic response in an idealized city. *Soil Dyn Earthquake Eng*. 2003;23(5):391-402.

34. Uenishi K. The town effect: dynamic interaction between a group of structures and waves in the ground. *Rock Mech Rock Eng*. 2010;43(6):811-819.

35. Tu T, Yu H, Ramirez-Guzman L, Bielak J, Ghattas O, Ma KL, O'Hallaron DR. From mesh generation to scientific visualization: An end-to-end approach to parallel supercomputing. In: *Proceedings of the* 2006 ACM/IEEE Conference on Supercomputing, 2006.

36. Guidotti R, Mazzieri I, Stupazzini M, Dagna P. 3D numerical simulation of the site-city interaction during the 22 February 2011 MW 6.2 Christchurch earthquake. In: *15th World Conference of Earthquake Engineering*. Lisboa, Portugal, 2012.

37. Steelman JS, Hajjar JF. Influence of inelastic seismic response modeling on regional loss estimation. *Eng Struct*. 2009;31(12):2976-2987.

38. Evangelista L, del Gaudio S, Smerzini C, et al. Physics-based seismic input for engineering applications: a case study in the Aterno river valley, Central Italy. *Bull Earthquake Eng*. 2017;15(7):2645-2671.

39. Smerzini C, Pitilakis K, Hashemi K. Evaluation of earthquake ground motion and site effects in the Thessaloniki urban area by 3D finite-fault numerical simulations. *Bull Earthquake Eng*. 2017;15(3):787-812.

40. Komatitsch D, Tromp J. Introduction to the spectral element method for three-dimensional seismic wave propagation. *Geophys J Int*. 1999;139(3):806-822.

41. Thomson W. *Theory of vibration with applications*. CRC Press; 1996.

42. Pan B, Xu JD, Haruko S, He HL. Simulation of the near-fault strong ground motion in Beijing region. *Seismol Geology*. 2006;28(4):623-634.

43. Fu CH. *A study on long-period acceleration response spectrum of ground motion affected by basin structure of Beijing*. Institute of Geophysics, China Earthquake Administration, Beijing, China: Dissertation; 2012.

44. Xie JJ, Zimmaro P, Li XJ, Wen ZP, Song YS. VS30 empirical prediction relationships based on a new soil-profile database for the Beijing plain area, China. *Bull Seismol Soc Am*. 2016;106(6):2843-2854.

45. Schnabel PB, Lysmer J, Seed HB. SHAKE: a computer program for earthquake response analysis of horizontal layered sites. In: *Earthquake Engineering Research Center (EERC) Report*. University of California at Berkeley; 1972.